The 21st International Congress on Sound and Vibration

13-17 July, 2014, Beijing/China

PREVENTING STROKE SATURATION IN PROOF-MASS ACTUATORS USING A DETECTION SCHEME

Laurence Wilmshurst, Maryam Ghandchi-Tehrani, Stephen Elliott

Institute of Sound and Vibration Research, University of Southampton, Southampton, UK SO17 1BJ

e-mail: lw5e10@soton.ac.uk

Proof-mass actuators are highly advantageous for active control applications, due to their large force-to-weight ratio. However, if the input voltage is large, the proof-mass will exceed the stroke length and hit the end stops, thereby imparting large impulses to the structure. This undesirable nonlinear phenomenon, known as stroke saturation, greatly reduces the closed-loop stability margin by accentuating regions of potential instability already present in the underlying linear closed-loop system.

In order to ensure closed-loop stability, a means of detecting stroke saturation is devised using an accelerometer placed on the actuator casing to generate a detection signal, which is used to activate or alter a feedback control loop. First, the dynamics of a Micromega IA-01 actuator are measured for the purpose of establishing an actuator model and to observe the impulses that occur as a result of stroke saturation. Next, the detection scheme procedure is outlined, where a detection signal is created using the impulses in the accelerometer signal. Finally, the detection scheme is implemented in a feedback loop to prevent stroke saturation by reducing the input gain to the actuator whenever stroke saturation occurs. This is demonstrated using a nonlinear actuator model in Simulink and an experimental setup.

1. Introduction

The ever-increasing demand for smart, lightweight structures in recent times has necessitated the use of active vibration control as a means of limiting structural vibration. Passive control methods are not effective at low frequencies and usually add mass to the structure, thereby conflicting with the requirements for lightness and flexibility. As an alternative control approach, the structural velocity or displacement is fed back to a collocated actuator in order to generate a control force, such that the effective stiffness or damping of the closed-loop system is increased in relation to the open-loop system [1].

Proof-mass actuators generate a control force by electromechanical means, where an inertial mass is accelerated in response to an input voltage, in order to provide a reaction force on the actuator casing. Although these actuators generally have a large force-to-weight ratio and do not require a ground reference to provide inertia [2], one significant drawback of their operation is that the displacement of the proof-mass is limited by the actuator stroke length, such that the inertial mass will collide with the end stops if the input voltage is large [3]. This phenomenon is known as stroke saturation, and is highly detrimental in control applications, since it can damage the actuator and destabilise the closed-loop system, as described by Baumann and Elliott [4]. For these reasons, it is desirable that additional control measures are taken whenever this phenomenon occurs.

In this study, an experimental scheme for detecting stroke saturation is devised by monitoring a signal from an accelerometer placed on the actuator casing, such that detection-dependent control can be applied. Recently, Wilmshurst et al. [5] demonstrated that, in principle, closed-loop destabilisation can be prevented by utilising detection-dependent control, which is extended in this paper by outlining the practical implementation of the detection scheme. Section 2 investigates the dynamics of a Micromega IA-01 proof-mass actuator [6] using experimental measurements and system identification techniques, as covered in [7]. Section 3 describes the detection scheme procedure using the measured accelerometer signals. Section 4 covers the implementation of the detection scheme in a feedback loop, where the velocity of the actuator is fed back to the control input for the purpose of reducing the input voltage whenever stroke saturation occurs. Conclusions and future work are stated in Section 5.

2. Dynamic Analysis of a Proof-Mass Actuator

By assuming that the proof-mass actuator behaves as a single-input single-output system on a rigid base, the general state-space equations for the actuator dynamics can be written as,

$$\dot{\mathbf{x}} = \mathbf{f(x)} + \mathbf{B}u \tag{1}$$

where $\mathbf{x} = [x_p \ \dot{x}_p]^T$ is the proof-mass displacement and velocity respectively, $\mathbf{f(x)}$ represents the internal actuator dynamics, accounting for nonlinear effects such as stroke saturation, $\mathbf{B}$ is the input matrix and u is the primary input signal. By considering the linear and nonlinear stiffness and damping forces separately, $\mathbf{f(x)}$ and $\mathbf{B}$ can be written as,

$$\mathbf{f(x)} = \begin{bmatrix} \dot{x}_p \\ \frac{-1}{m_p}(k_p x_p + c_p \dot{x}_p + f_{non}(x_p, \dot{x}_p)) \end{bmatrix}, \mathbf{B} = \begin{bmatrix} 0 \\ \frac{g}{m_p} \end{bmatrix} \tag{2}$$

Here, m_p is the mass of the internal proof-mass, k_p and c_p are the linear stiffness and damping terms of the actuator suspension, $f_{non}(x_p, \dot{x}_p)$ represents the nonlinear stiffness and damping forces due to stroke saturation, and g is the actuator gain.

In order to establish these dynamics, the actuator was attached horizontally to an approximately rigid steel block via a PCB 208 C01 force sensor, for the purpose of measuring the blocked force f_p of the actuator in response to an input voltage. Source generation and data acquisition tasks were performed in MATLAB through the use of a National Instruments NI-cRIO-9623 I/O module. The input voltage signal was amplified by a Micromega Dynamics Rack-04-45N prior to driving the inertial actuator, and the force sensor output signal was conditioned by a PCB ICP sensor signal conditioner. In addition, a Dytran 3035BG accelerometer was placed on the actuator casing to ascertain the acceleration-time signals of the actuator for the saturation detection scheme. This signal was conditioned by a Dytran 4102C sensor signal conditioner. The experimental setup is shown in Figure 1.

The time histories of the conditioned force sensor signal and the input voltage signal were recorded over a period of ten seconds, using a sampling rate of 51.2 kHz, to obtain the measured signals. These signals were obtained over a range of input frequencies from 5 Hz to approximately 50 Hz using stepped-sine excitation, whilst maintaining a constant excitation amplitude. The excitation frequency vector $\omega(n)$ used had a variable resolution, given by,

$$\omega(n) = 10\pi \cdot 1.02^{n-1} \tag{3}$$

where n is the index number, such that the resolution is greater at low frequencies.

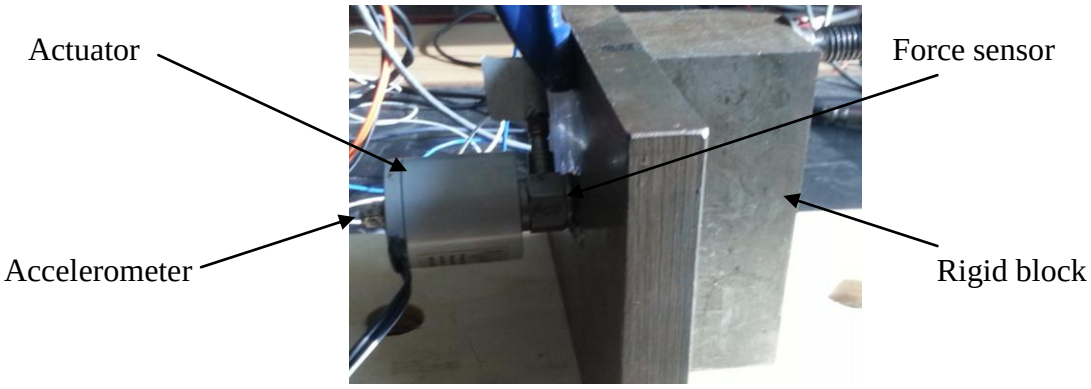

Figure 1: Illustration of experimental setup, including the actuator, force sensor, and accelerometer.

Initially, a small excitation amplitude $V_{in} = 0.1$ Volts was used to drive the actuator, in order to obtain the underlying linear displacement-voltage transfer function [5] of the actuator, denoted by $H(\omega)$, using the relation $x_p = -\omega^2 f_p / m_p$. Here, the mass $m_p = 0.032$ kg is known from the design specifications [6]. The rest of the linear system parameters were then identified from the measured transfer function using a curve-fitted model of the form,

$$H(\omega) = \frac{g}{k_p - m_p\omega^2 + j\omega c_p} \tag{4}$$

The identified parameters and the measured transfer function are shown in Figure 2.

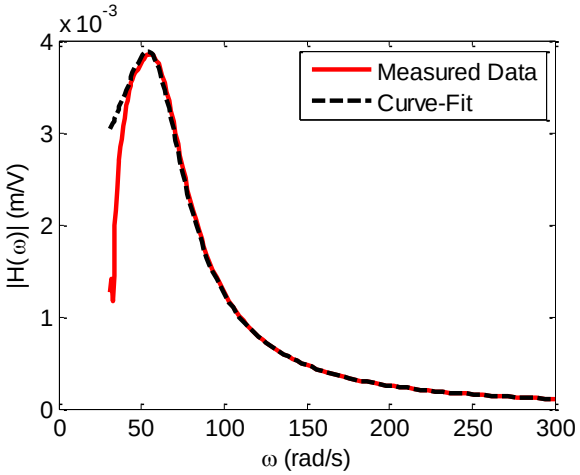

Figure 2: Measured displacement-voltage transfer function (solid) against the curve-fitted transfer function (dashed). The model parameters are $m_p = 0.032$ kg, $c_p = 1.3$ Ns/m, $k_p = 120.56$ N/m, $g = 0.3$.

To examine the nonlinear saturation dynamics $f_{non}(x_p, \dot{x}_p)$, the excitation amplitude was increased to $V_{in} = 0.4$ Volts and the measurement procedure was repeated. In this case, the excitation level was high enough to saturate the actuator, such that the proof-mass regularly came into contact with the end stops. Figure 3 shows one of the measured force-time histories, where it is apparent from impulsive shocks that stroke saturation occurs. By assuming that the end stops act as a spring with almost infinite stiffness, $f_{non}(x_p, \dot{x}_p)$ can be modelled as a simple hard-clipping saturation effect,

$$f_{non}(x_p, \dot{x}_p) = \begin{cases} k_{sat} x_p & x_p \geq |d| \\ 0 & x_p < |d| \end{cases} \tag{5}$$

where d is the stroke length, defined as $\pm 1\,\text{mm}$, and k_{sat} is the equivalent infinite stiffness associated with hard-clipping saturation.

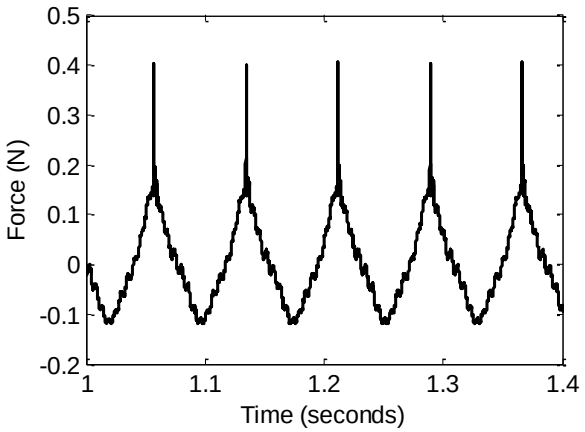

Figure 3: Measured force-time of the actuator for $V_{in} = 0.4$ Volts, $\omega = 26\,\text{rad/s}$.

3. Saturation Detection Scheme

The measurements conducted in the previous section indicate that the presence of stroke saturation results in large, narrow impulses in the force-time histories. Since the acceleration-time histories $\ddot{x}_p$ of the actuator are proportional to the force-time histories through $f_p = m_p \ddot{x}_p$ these impulses are also present in the accelerometer signal. Therefore, stroke saturation can be detected by monitoring the accelerometer signal and setting a threshold that indicates whether an impulse has occurred or not. Depending on the magnitude of the impulses, the impulse duration ranges from several hundred microseconds to about one millisecond, such that the spectral region associated with stroke saturation is 1 – 3 kHz; a band-pass filter is therefore utilised on the accelerometer signal to minimise background noise, remove the DC offset, and to focus on this spectral region.

In order to illustrate the abruptness of the onset of stroke saturation, the input amplitude V_{in} is slowly increased in increments of $0.01\,\text{Volts}$, starting at $0.4\,\text{Volts}$, until the impulses associated with stroke saturation appear in the acceleration-time signals. The filtered accelerometer signals, with the excitation frequency $\omega = 20\pi$ rad/s, are illustrated in Figure 4. At the lowest excitation amplitude $V_{in} = 0.4\,\text{Volts}$ stroke saturation does not occur, and therefore the accelerometer signal only contains background noise from the measurements. When the excitation amplitude was increased slightly to $0.41\,\text{Volts}$, impulses that are well above the background noise level start to appear in the force-time signals, thereby indicating that stroke saturation is present.

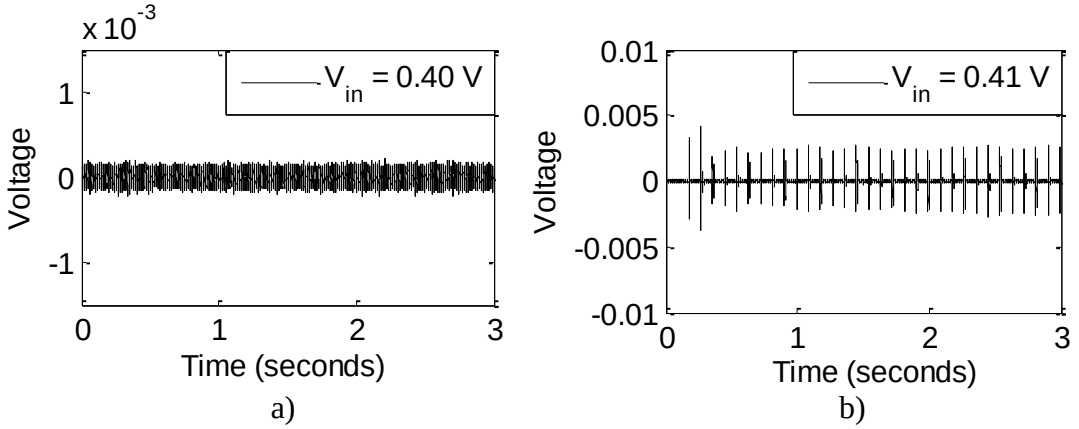

a) b)

Figure 4: Measured accelerometer voltage of the actuator at two similar excitation amplitudes.

Since the background noise level is consistent, it is possible to distinguish the impulses associated with stroke saturation by setting a threshold value $T = 10^{-3}$ Volts that the filtered acceleration-time signal $\ddot{x}_{filt}$ (in Volts) must exceed for stroke saturation to be detected. Here, $\ddot{x}_{filt}$ is used to create a detection signal x_{dec} that is unity when the threshold is exceeded and zero beneath the threshold,

$$x_{dec} = \begin{cases} 1 & |\ddot{x}_{filt}| \geq T \\ 0 & |\ddot{x}_{filt}| < T \end{cases} \tag{6}$$

In order to prevent chattering, where the detection signal switches rapidly between the on-off states when $\ddot{x}_{filt} \approx T$, a zero-order hold is utilized, such that the detection signal is held at unity for a specific number of samples N when stroke saturation is detected. This ensures that the controller is always active during stroke saturation. In this case, N is defined as 1000 samples.

There are a number of ways that the detection signal can be utilized in a control scheme. Firstly, it can be used directly as a gain in the feedback loop, such that the feedback control is active during stroke saturation. Alternatively, the detection signal can be used to incrementally increase the gain of the feedback loop whenever stroke saturation is detected, which is achieved by integrating x_{dec} before implementation as a feedback gain. This approach is advantageous in adaptive control, where, for example, the feedback control is used to steadily reduce the input excitation to the actuator until stroke saturation no longer occurs. A Simulink schematic of the saturation detection procedure is illustrated in Figure 5, using the accelerometer signal for detect saturation and to alter the gain of the control input used for the feedback loop.

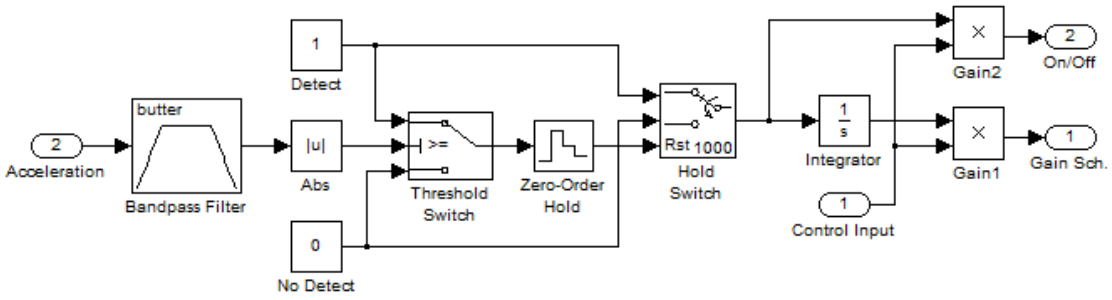

Figure 5: Implementation of detection scheme in Simulink, including filtering, detection, hold time, and integration.

Using the accelerometer signal in Figure 4b), the corresponding detection and gain scheduling signals obtained from the schematic in Figure 5 are shown in Figure 6a) and 6b) respectively.

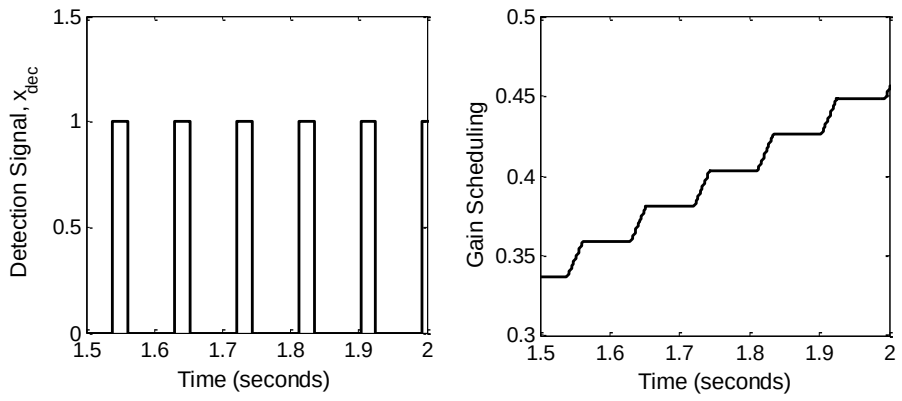

a) b)

Figure 6. Signals generated by the detection scheme for a) on-off and b) gain scheduling.

4. Detection-Dependent Control of an Inertial Actuator

4.1 Simulations

In this section, we demonstrate the use of the saturation detection scheme within a feedback loop for control purposes. Here, a simple pure-gain velocity-feedback loop is applied to the established nonlinear actuator model in Simulink, such that the effective damping of the actuator is increased when the control loop is active. An illustration of the Simulink model is shown in Figure 7.

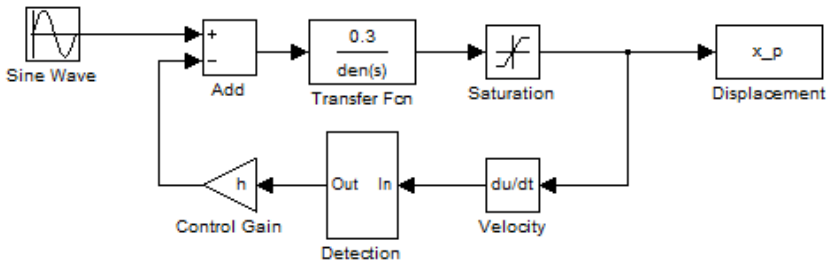

Figure 7: Simulink model of actuator with velocity feedback control and saturation detection.

The underlying linear closed-loop transfer function of the actuator $H_c(\omega)$ is given as,

$$H_c(\omega) = \frac{g}{k_p - m_p\omega^2 + j\omega(c_p + h_c)} \tag{7}$$

where h_c is the composite gain of the control gain h and the detection block gain h_{dec}. Provided that the excitation frequency ω is close to the peak resonance frequency $\omega_p \approx 65\,\text{rad/s}$ of the actuator, the relationship between the input excitation $V_{in}(\omega)$ and the actuator velocity $V_{vel}(\omega)$ is,

$$V_{vel}(\omega) = V_{in}(\omega)H_c(\omega) = \frac{j\omega g\, V_{in}(\omega)}{k_p - m_p\omega^2 + j\omega(c_p + h_c)} \approx \frac{gV_{in}(\omega)}{c_p + h_c} \tag{8}$$

such that the velocity signal is approximately in-phase with the input excitation. Therefore, the modified input excitation to the actuator $V_{in}(\omega) - h_c V_{vel}(\omega)$ is reduced in relation to $V_{in}(\omega)$, hence the apparent increase in damping.

Since the feedback control loop has the effect of reducing the input excitation, the detection scheme is used to apply gain scheduling within the feedback loop, such that the effective feedback gain h_c is increased whenever stroke saturation is detected. In this case, the measured accelerometer signal in Figure 4b) is used for detecting stroke saturation, and so the excitation frequency of the sine wave is specified as 20π rad/s. In this manner, the input excitation to the actuator is reduced when stroke saturation occurs, until the actuator response falls beneath the saturation threshold. Therefore, the effect of the detection block is to act as an adaptive feedback control gain that can react to small changes in the saturation threshold to ensure that stroke saturation does not occur.

Figure 8 illustrates the results of a simulation run over a period of three seconds, using a sine wave with an amplitude of $V_{in} = 1\,\text{Volt}$ and frequency $\omega = 20\pi\,\text{rad/s}$. In addition, the feedback control gain h was defined as 50. In Figure 8a), the input signal (i.e. the sum of the excitation and control signals) is shown with respect to the composite feedback gain h_c. Here, it can be seen that, initially, the input signal is severely distorted by the control signal when stroke saturation occurs. As h_c increases, the input signal reduces in amplitude and becomes less distorted, until a sinusoidal response is achieved. A comparison of the actuator responses, with and without control, is shown in Figure 8b). Whilst the uncontrolled response remains saturated, the controlled response gradually becomes less saturated until it falls beneath the threshold, thereby preventing stroke saturation.

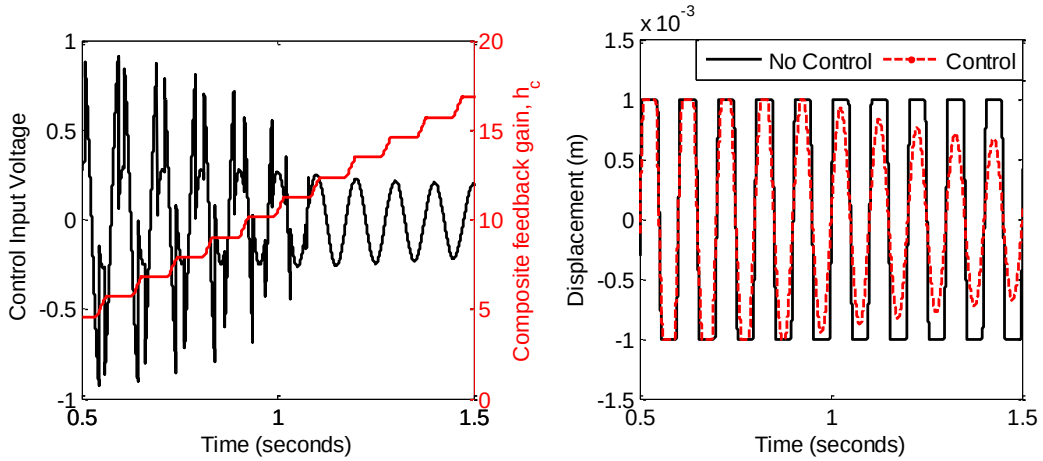

a) b)

Figure 8: Simulation results, with a) the actuator input and control gain, b) the actuator responses.

4.2 Experiments

In order to test the detection scheme in a practical environment, the Simulink schematic described in the previous subsection was modified and applied to the setup shown in Section 2 using a dSpace DS1103 Controller Board and ControlDesk. The modifications are as follows. Firstly, the continuous-time Simulink model was converted to discrete-time, using a sampling rate of 51.2 kHz. Secondly, an external signal generator is used to provide the sinusoidal excitation signal to the actuator, such that it cannot be directly affected in MATLAB. Thirdly, the actuator model is replaced by the physical actuator, where the digital inputs are the signals from the force and accelerometer sensors, and the digital output is the input excitation to the actuator. The force sensor signal is used to generate the velocity feedback signal by accounting for the proof-mass $m_p = 0.032\text{kg}$ and the sensor sensitivity $S = 110\text{mV/N}$ and applying discrete-time integration. Fourthly, in order to remove the DC offset of the force sensor to facilitate integration, the force-time signal is down-sampled to 1.28 kHz, such that a high-pass filter can be used to remove the DC offset without affecting the low-frequency excitation signal. The resulting control signal was then up-sampled to 51.2 kHz before summation with the excitation signal. Additional anti-aliasing and reconstruction filters were required for this purpose. Finally, a saturation block of 30 was applied to the composite feedback gain to limit the control signal and prevent damage to the actuator if closed-loop destabilisation occurs.

Figure 9 illustrates the detection-dependent control of the actuator using an excitation signal of amplitude $V_{in} = 0.4\text{Volts}$ and frequency $\omega = 20\pi$ rad/s, control gain $h = 2$ and threshold $T = 10^{-3}$ Volts. Here, it can be seen that the impulses in the accelerometer decrease as h_{dec} increases

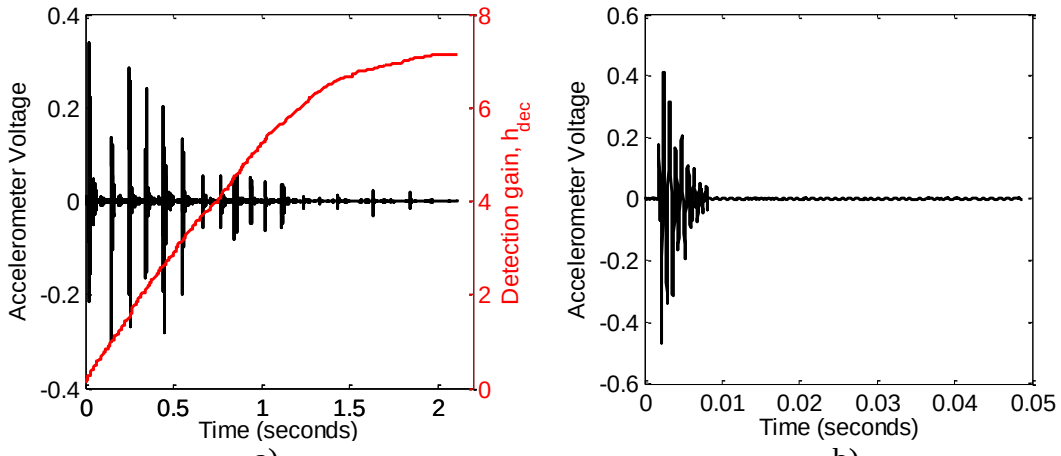

a) b)

Figure 9: Measurements a) Accelerometer signal and detection gain, b) Impulse response, $h = 2$.

until stroke saturation no longer occurs. In addition, the closed-loop response to a hammer impulse is shown in Figure 9b), which demonstrates that the system remains stable. By increasing the gain to $h = 15$ and repeating the procedure, as shown in Figure 10, the controller prevents stroke saturation at a faster rate, but the closed-loop system is prone to instability, as the limit-cycle oscillation in Figure 10b) shows. Therefore, choosing h is a trade-off between performance and robustness.

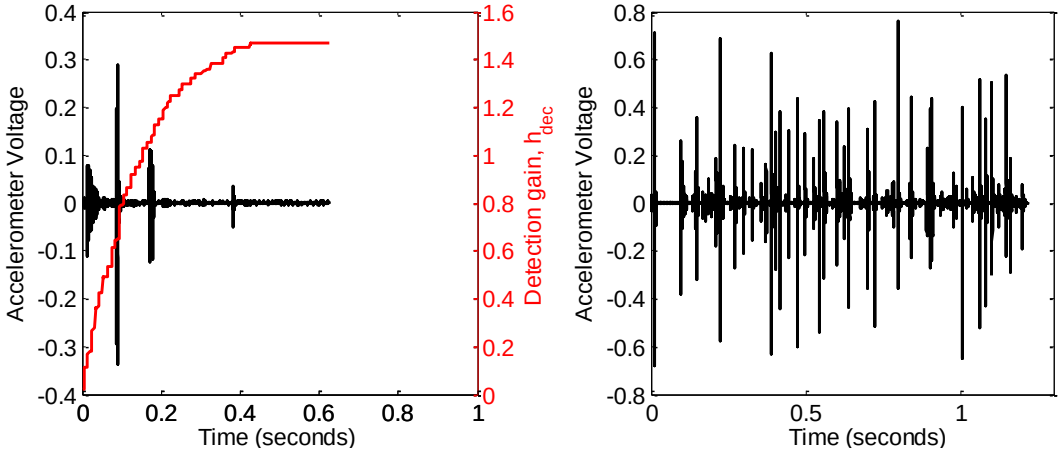

a) b)

Figure 10: Measurements a) Accelerometer signal and detection gain, b) Impulse response, $h = 15$.

5. Conclusions

A simple control scheme for detecting stroke saturation in inertial actuators using an accelerometer signal is presented, using a Micromega IA-01 actuator as an exemplary case. The detection scheme is applied in a velocity feedback loop, such that the control gain increases adaptively when stroke saturation is detected. In this case, the detection-dependent feedback control is generally effective at preventing stroke saturation, although the closed-loop system may become unstable if the initial control gain is too high. This is confirmed using simulations and experimental data.

Future work will focus on applying the detection scheme to an actuator that is attached to a flexible structure, where the detection scheme can be utilised to deactivate the control loop when stroke saturation occurs, to prevent closed-loop destabilisation. In addition, alternative measures of detecting stroke saturation from the accelerometer signal will be considered, such as analysing the crest factor or kurtosis, in order to improve the consistency of the detection process.

REFERENCES

1. Neild, S. and Wagg, D. A. (2010) *Nonlinear vibrations with control: for flexible and adaptive structures*, Springer, New York
2. Berlin, A. A., Chase, J. G. and Yim, M. Integrated centering control of inertially actuated systems, *Control Engineering Practice*, **7**(9), 1079-1084, (1999).
3. Borojevic, D., Lindner, D. K. and Zvonar, G. A. Performance and control of proof-mass actuators accounting for stroke saturation, *Journal of Guidance, Control, and Dynamics*, **17**(5), 1103-1108, (1994).
4. Elliott, S. J. and Baumann, O. N. Destabilization of velocity feedback controllers with stroke limited inertial actuators, *Journal of the Acoustical Society of America*, **121**(5), 211-217, (2007).
5. Elliott, S. J., Ghandchi-Tehrani, M., and Wilmshurst, L. I. Active control and stability analysis of flexible structures using nonlinear proof-mass actuators, *Eurodyn 2014:IX International Conference on Structural Dynamics*, (2014).
6. Micromega Dynamic: Active Damping Devices and Inertial Actuators. [Online.] available: http://www.micromega-dynamics.com/doc/ADD_Catalog_Rev2.pdf
7. Elliott, S. J., Ghandchi-Tehrani, M., and Wilmshurst, L. I. Nonlinear vibrations of a stroke-saturated inertial actuator, *11th International Conference on Recent Advances in Structural Dynamics*, (2013).